X-Ray Radioluminescence in Diversely Doped Multimode Silica-based Optical Fibers

Arnaud Meyer, Adriana Morana, Hicham El Hamzaoui, Bruno Capoen, Geraud Bouwmans, Mohamed Bouazaoui, Sylvain Girard, Emmanuel Marin, Youcef Ouerdane, Aziz Boukenter

X-Ray Radioluminescence in Diversely Doped Multimode Silica-based Optical Fibers

Arnaud Meyer, Adriana Morana, *Member IEEE*, Hicham El Hamzaoui, Bruno Capoen, Géraud Bouwmans, Mohamed Bouazaoui, Sylvain Girard, *Senior Member, IEEE*, Emmanuel Marin, Youcef Ouerdane and Aziz Boukenter

***Abstract*—The radioluminescence response under X-rays is investigated for five different types of multimode silica-based optical fibers doped with Ge, P, Al, F or Ce. The results indicate that all tested fibers show a measurable radioluminescence signal at dose rates from 0.1 to 15 Gy(SiO_2)/s, using 10-cm-long samples and a photomultiplier-based acquisition chain. Other influences of radiation, such as radiation-induced attenuation, are discussed in order to evaluate the potential of such fiber types for radiation detection or dosimetry applications.**

***Index Terms*—Optical fiber, Radiation, Dosimetry, Radioluminescence, Scintillators.**

I. Introduction

Optical fibers (OFs) are waveguides well-suited for radiation monitoring because of their ability to act both as a sensing element and as a means of transporting measurement signal to devices located outside of the radiation area. Radiation effects on OFs can be mainly categorized into three different phenomena [1]: radiation-induced attenuation (RIA), which causes transmitted signal to decrease, radiation-induced emission (RIE), which consists of a measurable signal to be emitted during and/or after irradiation, and radiation-induced refractive index change (RIRIC), which causes a modification of the refractive index of either OF core or cladding material.

Amidst phenomena linked with RIE, radioluminescence (RL), ie. emission induced by exciting, through irradiation, defects created during the fiber manufacturing and/or radiation-induced point centers, is particularly of interest, because the produced signal is conveniently transmitted by the optical fiber producing the RL signal. The emitted light is then relatively easy to measure using conventional optical devices such as photomultiplier tubes.

OF-based scintillators have been widely studied and are commonly used for dosimetry purposes, especially in the medical area. Usual materials for this type of application typically involve specially engineered crystals or plastics [2], which yield a high RL signal, but are not designed to operate at high levels of total ionizing dose (TID) or high dose rates that could be encountered in severe environments such as space, nuclear or high-energy physics facilities.

Rods or OFs, optimized for dosimetry through measurement of RL signal, have been produced and studied, and typically involve dopants such as cerium (Ce) [3], [4], gadolinium (Gd) [5] or copper (Cu) [6], which are less commonly employed in commercially available optical fibers.

However, previous studies [7] have shown that OFs with more commonly available dopants may also show significant RL signal. We investigate in this study the RL properties of a panel of OFs, in order to assess their potential for dosimetry applications as sensing elements.

II. Materials and Methods

A. Choice of samples

Five different types of multimode optical fibers, listed in Table I, were selected for this study, based on multiple criteria: their availability, to evaluate well-known kinds of fiber that are used on common applications, their already known properties under radiation, ranging from radiation-hardened to radiation-sensitive, and their composition. All samples share a same structure, with pure silica in the cladding (except for F-doped fiber) and pure silica doped with a single dopant in the core. Finally, multimode OFs were selected because of their larger core diameter, and therefore increased sensitive volume, compared to single-mode OFs.

Table I
Optical fiber samples used for this experiment

Symbol	Core dopant	Core diameter	Manufacturer	Length ± 1 mm
Ge	Germanium	62 µm	iXblue	10 cm
P	Phosphorus	62 µm	iXblue	10 cm, 1 cm
Al	Aluminum	42 µm	iXblue	10 cm, 1 cm
F	Fluorine	50 µm	Draka	10 cm
Ce	Cerium	40 µm	FiberTech Lille	1 cm

Germanium (Ge) is amongst the most commonly available dopants for optical fibers, and the one primarily used for optical fiber-based telecommunication. The sample chosen for this experiment is from a so-called “canonical” fiber [8], i.e. an optical fiber designed for research, reflecting the manufacturing process and properties of commercially-

Submitted on October 08, 2021; last revised on December 14, 2021

A. Meyer, A. Morana, S. Girard, E. Marin, Y. Ouerdane and A. Boukenter are with Univ Lyon, UJM-Saint-Etienne, CNRS, Institut d Optique Graduate School, Laboratoire Hubert Curien UMR 5516, F-42023, Saint-Étienne, France (e-mail: sylvain.girard@univ-st-etienne.fr).

H. El Hamzaoui, B. Capoen, G. Bouwmans, M. Bouazaoui are with Univ-Lille, CNRS, UMR 8523-PhLAM-Physique des Lasers Atomes et Molécules, F-59000 Lille, France (e-mail:mohamed.bouazaoui@univ-lille.fr).

available Ge-doped optical fibers. Previous studies of this fiber have highlighted a high cathodoluminescence (CL) signal [9], [10]. In particular, CL signal centered at ~400 nm was associated with Germanium Lone Pair Centers (GLPC), known to be natively present in as-drawn Ge-doped fibers. Such GLPC centers can be converted to Ge(1) and Ge(2) defects during irradiation [1], when the core of the sample is irradiated with 10 keV electrons [10]. Ge-doped fibers are abundantly studied for dosimetry applications, through RL although at lower doses to fit requirements for medical applications [11]–[13], and through thermoluminescence at higher TIDs [14]–[16].

Phosphorus (P) -doped fibers are known to show high RIA response, especially in the visible domain [17]. The sample chosen for this experiment is from another canonical fiber, which presented a very weak CL emission band, centered at ~410 nm and associated with P-related defects [10]. It should also be noted that a previous work showed that P-doped fibers could produce a RL signal exploitable for dosimetry under short (≤ 100 ms) X-ray pulses [18].

Aluminum (Al) is generally used as a codopant for Erbium-doped optical fiber amplifiers as it prevents undesirable clustering of rare-earth ions [19]. Similarly to P-doped OFs, Al-doped fibers also exhibit high RIA response [20]. A noticeable difference between P- and Al- doped fibers is their intrinsic, pre-irradiation transmission in the ultraviolet domain; the former being more transmitting whereas the latter is more absorbing. The Al-doped sample chosen for this experiment is a fiber sample designed by iXblue to study radiation response of Al-doped fiber without other dopants. CL measurements have shown an intense luminescence in the Al-doped core at ~380 nm [21].

Fluorine (F), on the opposite, is a dopant mainly used in radiation-hardened optical fibers. It decreases the refractive index of silica and is, consequently, generally present in the fiber cladding and in lesser concentration, or absent, in the fiber core. F-doped silica fibers, along with pure silica-core fibers, are the most radiation-hardened OFs known to date for steady-state radiation environments up to 100 kGy [22]. The sample chosen for this experiment is a commercially available "rad-hard" optical fiber, designed to yield very low RIA in both infrared and visible spectral regions. This same type of fiber is also used in our experiment as a transport fiber, to carry the RL signal of all tested samples outside of the irradiation chamber, to the acquisition system. CL measurements on this type of fiber shows luminescence bands centered at ~460 nm, ~560 nm and ~650 nm, similar to the one recorded in the pure silica cladding of other fibers [10]. A comparable type of fiber, with pure silica core and fluoropolymer cladding, was shown to exhibit under 100 – 225 MeV protons a RL signal with two bands also centered at ~460 nm and ~650 nm [23].

Finally, Cerium (Ce) doping was studied, since Ce-related centers present a strong RL signal at ~500 nm, often investigated for dosimetry applications [3], [4], [24]–[26]. A Ce-doped fiber sample developed and supplied by FiberTech Lille was included in this experiment in order to compare performances of the other samples against fibers designed and optimized for RL.

B. Measurement setup

All measurements were carried out at room temperature in the LabHX X-ray irradiator located in the Laboratoire Hubert Curien of Université Jean Monnet, Saint-Étienne (France).

The source of the irradiator is a COMET MXR 225/26 X-ray tube, using a tungsten anode driven at 100 kV, yielding X photons with a mean energy of ~40 keV and an adjustable dose rate, set by varying the tube filament current.

The setup used for measuring RL signal is depicted in Fig. 1a and involves a Hamamatsu H7421-40 photon counting head, which uses internally a photomultiplier tube with a GaAsP photocathode and works in a spectral range from 380 to 720 nm. It was installed outside of the irradiation chamber, inside a box designed to screen most of ambient light. Its integration time was set to 1 ms for these experiments.

To measure RIA and RL spectra, another setup, shown in Fig. 1b, involves an Ocean Optics DH-2000-BAL deuterium-halogen light source, covering a broad range of wavelengths from 210 nm to 2500 nm, and an Ocean Insight QE Pro spectrometer, operating between 250 nm and 1000 nm. The same setup, without switching on the light source, was used to acquire RL spectra of each sample.

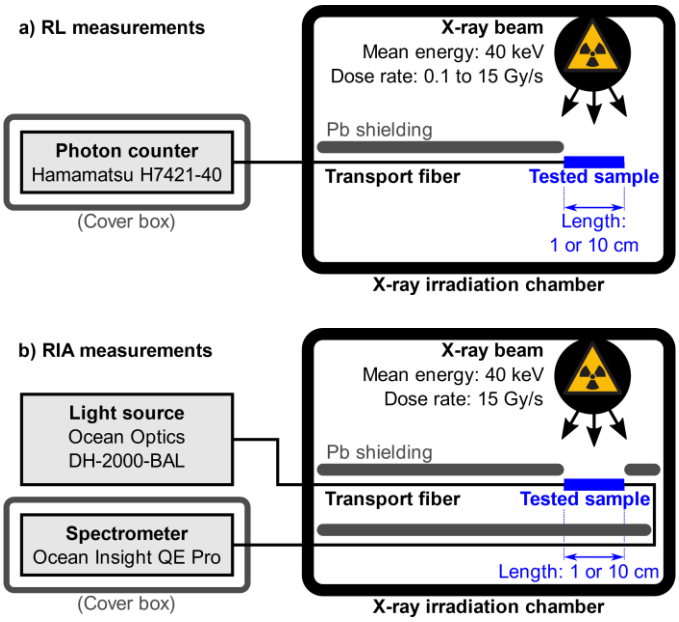

Fig. 1. Experimental setups. a) Setup for RL measurements. b) Setup for RIA measurements.

In order to transmit the RL signal emitted by the samples, a radiation-hardened optical fiber was spliced to each of the samples, one at a time. This transport fiber was of the same type as F-doped samples investigated in this work.

As preliminary results showed that this rad-hard fiber produces a non-null RL signal when exposed to X-rays, the transport fiber was shielded using 3 mm thick lead (Pb) plates, covering most of the transport fiber length inside the irradiation chamber until the splicing point with the sample under test.

Each of these samples was prepared at the length specified in Table I. Because of the very high RL signal of this fiber type, the Ce-doped sample was cut to a length of 1 cm in order not to saturate the detector. In the same way, to stay within the dynamics of the measuring system, RIA measurements on the more radiosensitive Al- and P-doped fibers were performed on samples of 1 cm long.

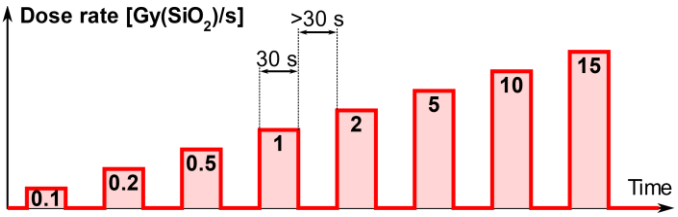

Fig. 2. Sequence of dose rates applied for irradiating each sample during RL measurements.

For RL measurements, each sample was irradiated according to a sequence of irradiations with a duration of 30 s each, followed by a pause of at least 30 s, for 8 values of dose rate from 0.1 to 15 Gy(SiO_2)/s (±10 %), as shown in Fig. 2. The X-ray tube filament current was set from 0.15 to 25 mA in order to reach these dose rate values.

Total dose deposited on the sample is accumulated between subsequent dose rates and reaches ~1.0 kGy at the end of the sequence. Therefore, effects of TID must be considered along with dose rate, especially for radiation sensitive optical fibers.

For RIA and spectral RL measurements, fresh samples were irradiated 10 times for 30 s at a single dose rate value of 15 Gy(SiO_2)/s (±10 %), with a pause of at least 30 s between each irradiation.

C. Data analysis

For RL measurements, the measured photon counts during irradiation were summed in bins of 1 s and subtracted with the mean dark signal measured just before irradiation start, for each tested sample.

For spectral RL measurements, all spectra were subtracted with the dark signal measured prior to each run, and scaled using the spectral response of the whole measurement chain from a calibrated halogen source.

For RIA measurements, all transmission spectra were subtracted with the dark signal measured prior to each run, and parasitic signal in the UV domain was compensated by subtracting from each spectrum its mean value measured between 250 and 260 nm.

D. Repeatability of RL measurements

In order to evaluate the uncertainties linked to our setup, 4 similar RL runs have been performed on 10 cm-long Al-doped samples, irradiated during 30 s at a dose rate of 10 Gy(SiO_2)/s (±10 %). For each run, the new sample was positioned and spliced to the transport fiber, and the connection of the other end of transport fiber to the photon counting device was performed anew.

By analyzing the difference in photon counts between these 4 runs, depicted in Fig. 3, we determined an overall uncertainty of ± 25 % on the measured RL signal. This is explained by variabilities of sample length, splice quality between sample and transport fiber, and quality of signal injection in the photon counting device.

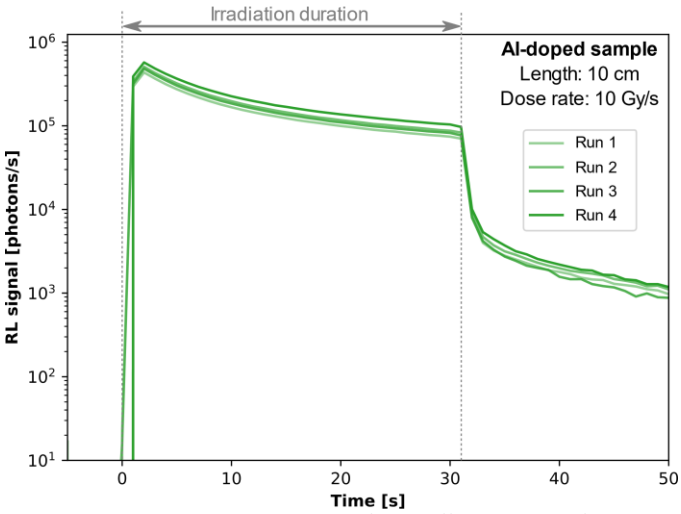

Fig. 3. RL signal over time recorded for 4 different pieces of Al-doped sample, irradiated each during 30 s at a dose rate of 10 Gy/s in order to check the variability of our measurement setup.

III. Results and Discussion

A. RL signal against time

An example of time traces of measured RL signal of a single sample, the 10-cm-long Ge-doped fiber, is shown in Fig. 4. This type of graph clearly illustrates that the higher the dose rate, the higher the intensity of measured RL signal. Moreover, in case of radiosensitive samples, such as the depicted Ge-doped fiber, we can also observe that the RL signal intensity decreases with irradiation time, particularly at higher dose rates.

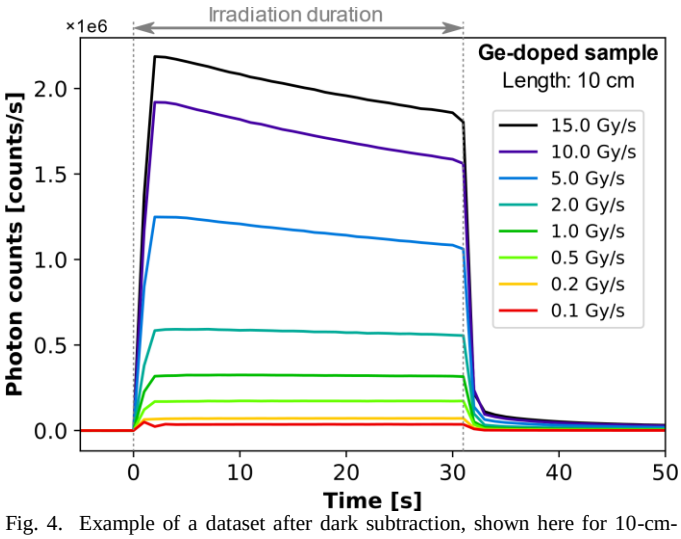

Fig. 4. Example of a dataset after dark subtraction, shown here for 10-cm-long Ge-doped sample. Time origin has been defined at irradiation start for each run.

Because our setup involves low energy (≤ 100 keV) X rays, there is no significant occurrence of Cherenkov effect and therefore its influence on RL signal was not evaluated in the

scope of our study.

Fig. 5 reports a comparison of all measured data at the highest investigated dose rate of 15 Gy/s. We can observe that the RL signal at this dose rate spreads roughly from 5×10^3 to 3×10^6 counts/s over the tested samples.

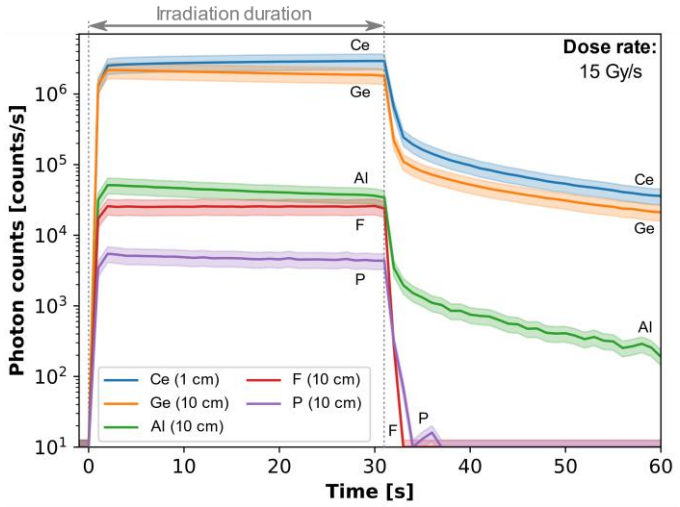

Fig. 5. Comparison of RL response of all tested fiber samples as a function of time, at the maximum dose rate of 15 Gy/s. Values lesser than 10^1 were clipped for clarity. Filled areas show the uncertainty range of ± 25 %.

Out of all fibers tested in our panel, the Ce-doped sample, even with a length of only 1 cm and the smaller sensitive volume, still delivers the most intense RL signal, which also noticeably increases during irradiation. The 10 cm-long Ge-doped sample also delivers an intense RL signal comparable to the Ce-doped one, despite the size, and therefore sensitive volume, difference of both samples.

On the other end of the range, the Al- and F-doped samples show a significant amount of RL, but at least one order of magnitude lower compared to previous samples at the highest tested dose rate. Finally, the P-doped sample stands out, as its measured RL signal is even lower than that of the F-doped fiber used for transport.

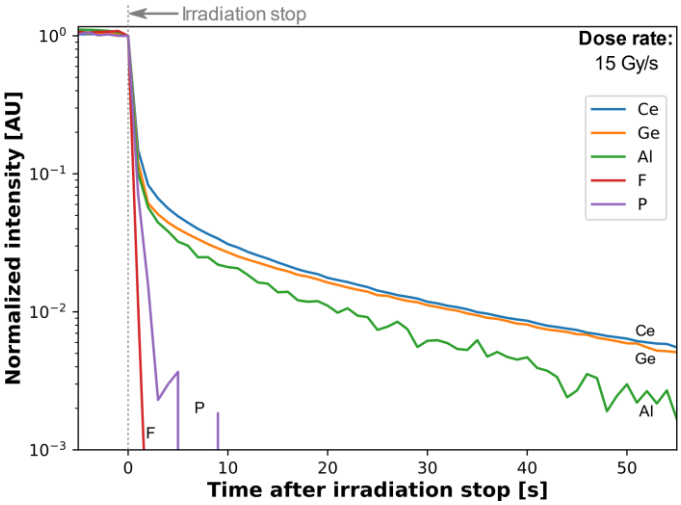

Fig. 6. Comparison of RL afterglow at 15 Gy/s of all tested fiber samples, normalized by the intensity measured at the end of irradiation. Values lesser than 10^3 were clipped for clarity.

The afterglow, i.e. remaining RL signal after irradiation, is shown in greater detail in Fig. 6, normalized for all samples by their RL signal measured at time of irradiation end. Afterglow is clearly identifiable for Ce-, Ge- and Al-doped samples, whereas it appears to be either absent, or too low in comparison to measurement noise, for F- and P-doped samples. When normalized, it appears that the afterglow response is very similar among Ce-, Ge- and Al-doped samples, decreasing to ~10 % and 1 % of original value respectively after 1 s and 30 s.

It is interesting to note that these RL results are in good agreement with the ones previously observed under CL experiments [10], despite very different irradiation conditions (X-rays versus electrons and low versus high dose rate). Particularly, the case of F- and P-doped samples sharing the same afterglow features suggests that, also for RL, Si-related defects could be involved. One important difference between CL and RL results however involves the possible impact of RIA on the RL fibers, even for low probe lengths, which is negligible in CL measurements.

B. Spectral features of RL signal

Measured RL spectra of Ce-, Ge- and Al-doped samples, calibrated as explained in section II.C, are shown in Fig. 7, normalized by integral to compare their shapes. Because of the low RL signal delivered by F- and P-doped samples, our setup was unable to measure a significant RL spectrum for these two samples.

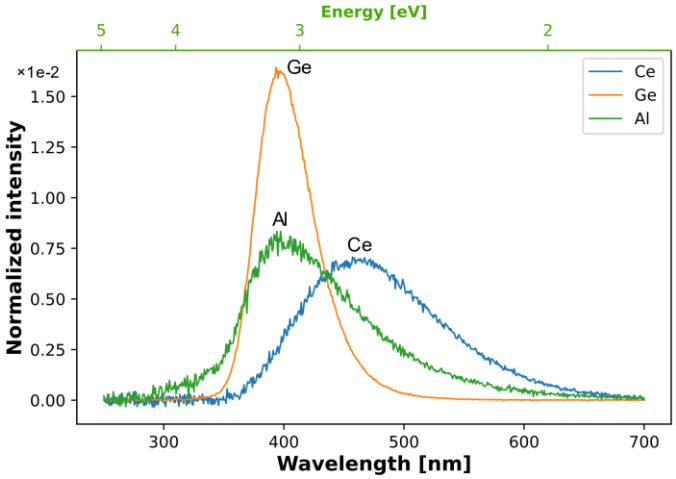

Fig. 7. RL spectra of Ce-, Ge- and Al-doped samples, integrated during 1 s between 0 and 15 Gy at 15 Gy/s, normalized by integral.

For the Ce-, Ge- and Al-doped samples, at least 95 % of the RL signal is emitted between 300 nm and 600 nm. The RL spectrum of the Ce-doped sample is centered at 2.6 eV and has been associated with 5d–4f transition of Ce^{3+} ions [3]. For the Ge-doped sample, the RL spectrum is centered as 3.2 eV, associated with GLPC [27], [28]. Finally, the underlying physical origins of the RL spectrum of Al-doped sample, centered at ~3.1 eV, are still discussed [21], as different mechanisms for this emission have been proposed; some attributing it to electron-hole recombination near Al-M^+ centers [29], others associating it with charge-compensated substitutional Al^{3+} (Al^{3+} – M) [30].

Fig. 8 shows the evolution of Ge-doped sample RL spectrum during irradiation. It illustrates that two phenomena influence RL signal during irradiation: a decrease in amplitude, as well as a change of the spectral shape of the emitted signal. While the former could be explained both by RIA and a decrease of the population of RL-inducing defects, such as GLPCs for the depicted Ge-doped sample, the latter could only be explained by a change in the spectral absorption of the fiber, and therefore only to the occurrence of RIA. Similar spectral evolution was also observed for the two other samples; in these cases, RIA is assumed to be the main factor for RL decrease.

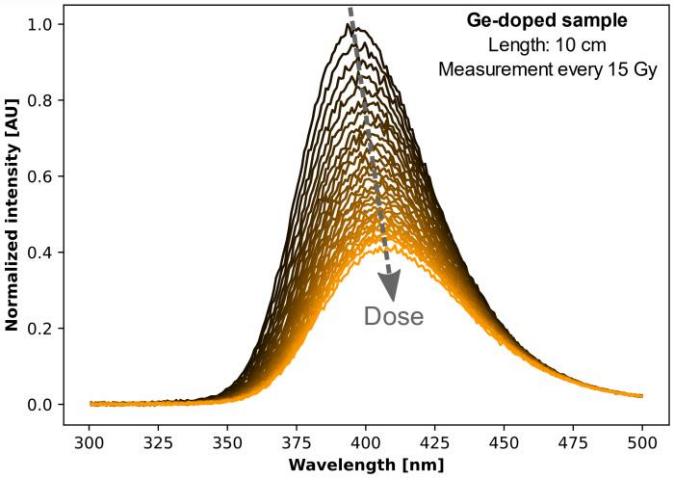

Fig. 8. Evolution of RL spectrum of Ge-doped fiber during irradiation. Each spectrum was acquired during 1 s at a dose rate of 15 Gy/s, amounting to a TID of 450 Gy at the end of the depicted sequence.

Also, because of the high sensitivity of Al-doped fiber to RIA, even more at shorter wavelengths as demonstrated in section 0, we may assume the Al spectrum shown in Fig. 7, acquired between 0 and 15 Gy, is affected by the occurrence of RIA and probably slightly shifted to the larger wavelengths.

C. *Radiation-induced attenuation (RIA)*

Because of their different compositions, the samples under test exhibit very different levels of RIA. Fig. 9 reports the measured RIA of all samples. Fig. 9a shows the spectral RIA measured after a single run of 30 s at 15 Gy/s, totaling to a TID of 450 Gy. Fig. 9b shows the evolution of RIA at 450 nm wavelength over TID up to 4.5 kGy.

The RIA response is very different amongst tested samples. Whereas, in Fig. 9a, F- and Ce-doped samples exhibit a comparatively low level of RIA over the whole measured spectrum, Ge-, P-, and Al- doped samples yield a high RIA in the short wavelengths region, where most of the RL signal appears to be emitted, which explains the decrease in amplitude as observed in Fig. 8. The fact that the RIA is not flat over the whole spectrum also explains the change of spectral shape observed in Fig. 8.

RIA kinetics shown in Fig. 9b further elaborate on the ample difference in RIA response between samples. While Ce- and F- doped fibers show little increase and a comparatively low RIA, Ge-, P- and Al-doped samples see a visible increase to high levels of RIA.

It is important to notice that the decrease in RL signal cannot be directly deduced from the measured RIA level, because each length element of the irradiated fiber emits a RL signal which travels through a different thickness of absorbing medium. A model taking into account these effects could be the goal of future studies and should allow to optimize the design of dosimeters.

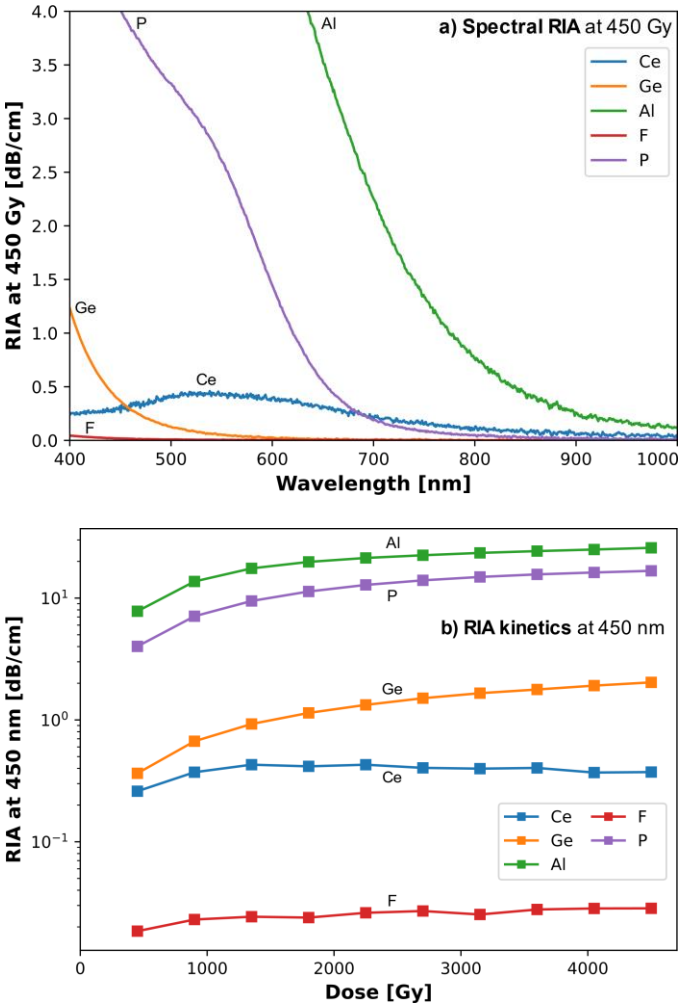

Fig. 9. RIA of all samples. a) Spectral RIA recorded at a TID of 450 Gy. b) Evolution of RIA at 450 nm as a function of TID.

D. *RL signal against dose rate*

To assert the dosimetry performance of all tested samples, the mean value of the RL signal produced during irradiation was calculated for all samples at all dose rates and plotted in Fig. 10a. We observe that all tested samples show a significantly measurable RL signal down to the lowest investigated dose rate of 0.1 Gy/s.

Whereas the characteristic of an ideal dosimeter would involve a delivered signal strictly proportional to the dose rate, comparison between data points and linear guidelines depicted in Fig. 10a shows that not all measured samples satisfy these requirements.

The Ge-doped sample shows excellent RL performances, as

the signal delivered by the 10-cm-long Ge-doped sample is greater than the 1-cm-long Ce-doped sample at low dose rates. However, this behavior changes at higher dose rates and the amount of RL signal appears to be decreasing compared to an expected linear extrapolation. This can be explained by two phenomena: the occurrence of RIA at the emission wavelengths, and the decrease during irradiation of the population of pre-existing GLPC defects, that are converted by radiation into Ge(1) and Ge(2) defects [27], [28].

The RIA effect is even more evident on the Al-doped sample, which high radiation sensitivity is well shown in Fig. 9. Because of the RIA increase with TID, dependence of RL signal of Al-doped sample with dose rate could not even be observed at the highest dose rates.

Similar conclusions can be drawn for the P-doped sample: although it appears to produce a signal comparable to F-doped fiber at low dose rates, its high RIA sensitivity results in a significantly decreased signal at higher dose rates.

On the opposite, the RL signal observed on the F-doped fiber sample presents a linear dependence on the dose rate, owing to its low RIA.

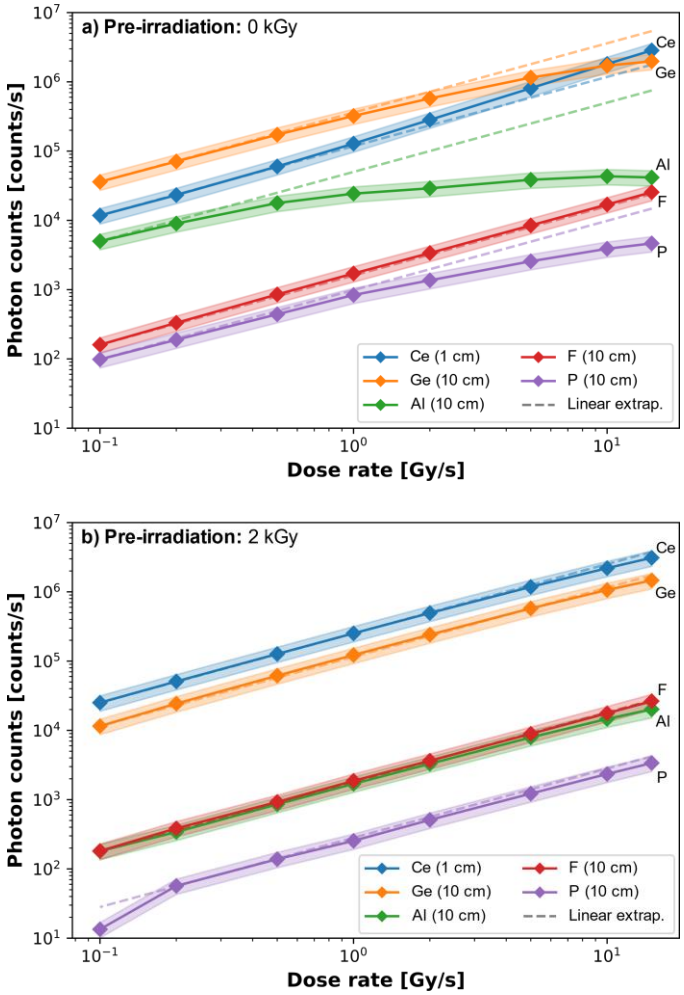

Fig. 10. Comparison of the mean value of RL signal of all tested fiber samples at different dose rates. Dashed lines show linear extrapolations from the first measurement points, in order to evaluate visually the linearity of each curve.
a) Results of the first run without pre-irradiation. b) Results of the third run, totaling a pre-irradiation dose of ~2 kGy. Filled areas show the uncertainty range of ± 25 %.

Finally, for the Ce-doped sample, the RL signal is noticeably increasing during irradiation, due to its RIA slowly decreasing with TID as shown in Fig. 9b.

In an attempt to mitigate the observed effects of RIA on the linearity of RL response on radiosensitive samples, an identical series of measurements was performed on pre-irradiated samples, obtained by repeating three times in a row the irradiation sequence described in Fig. 2. The results shown in Fig. 10b were obtained during the third run, therefore on samples pre-irradiated with a TID of 2 kGy.

As suggested by the RIA kinetics shown in Fig. 9b, RIA stabilizes as TID increases, and therefore the difference in attenuation between start and end of the run becomes less and less important. This is observed on the RL signal measured on pre-irradiated samples shown in Fig. 10b, where the non-linearities observed for Ge-, Al- and P-doped samples are significantly reduced, making these pre-irradiated samples more befitting for dosimetry applications. This increase in stability and reproducibility is however done at the expense of signal level, made evident by comparing Fig. 10a and Fig. 10b, and therefore a potentially degraded signal-over-noise ratio.

E. Potential for dosimetry applications

Whereas an ideal dose-rate meter would exhibit a constant ratio between dose rate and measured signal, the RL signal output by the fibers evaluated in this study depends on both dose rate and TID, as shown in the previous section. Therefore, dosimetry applications involving these fibers would have to take into account this dependence on TID.

A first solution would be for the operating electronics to compensate the effects of TID on the signal. This would involve either measuring a two-dimensional calibration function according to both dose rate and TID, or establishing a model of the evolution of dose rate sensitivity according to TID. In both cases, the system would need to store a measurement of the TID received by the sensor, taken either by an external dosimeter, or by integrating the measured dose rate after compensation (probably at the cost of a higher uncertainty level).

A second solution would be to pre-process the measuring elements in order to minimize the influence of TID on their sensitivity. This solution is explored in this study through the effects of pre-irradiation described in section III.D.

A last solution would be to consider the actual requirements of the target dosimetry application. Not all applications involve the full range of dose rates, TID and accuracy explored in this study. Medical imaging applications, for instance, usually involve much lower dose rates and TID than the ones we considered [31], resulting in a lesser influence of TID on the measurement that, if ignored, could result in an uncertainty range that may be acceptable.

IV. Conclusion

All multimode optical fibers tested in this study did show a significant, measurable RL signal in a range of dose rates from 0.1 to 15 Gy(SiO_2)/s.

The intensity of RL signal was shown to be increasing with dose rate in all cases. However, depending on the doping, RL intensity does not depend linearly on dose rate because of RIA, as well as possible defects generation and recombination mechanisms.

Spectral measurements in Ce- and Ge-doped samples have shown that the origins of RL signal is well understood for these two kinds of fiber, but much less for Al-doped fiber. The low intensity of RL signal emitted by F- and P-doped samples did not enable its spectral measurement, and therefore also makes it more difficult to reach a better understanding of the origins of such signal. However, the P-doped fiber noticeably delivers a RL signal significantly lower than the pure silica core F-doped fiber, hinting that P-doping may not be producing any kind of RL on its own in the UV-visible range of wavelengths that was explored in our study.

In particular, OFs sensitive to RIA, such as Al- or P-doped fibers, yield a RL signal which is very dependent on the total amount of received dose. This dependence can be mitigated by pre-irradiating the samples, as shown here with a pre-irradiation TID of 2 kGy(SiO_2), however at the cost of a decreased signal. Due to recovery over time of radiation-induced defects, the lifetime of such pre-irradiation need to be investigated.

In dosimetry applications, the preference would tend towards sensing elements with high sensitivity to dose rate, i.e. a strong RL signal, and low sensitivity to total dose, i.e. a low RIA and steady generation of RL-producing defects. Whereas OFs specifically designed for RL, such as the Ce-doped sample clearly show better suitability in both these parameters, we observe that Ge-doped fiber also yields significant amount of RL signal, despite being more sensitive to total dose, and that F-doped fiber has very low RIA, which makes it reliable at higher doses, despite having a significantly weaker RL signal.

Optical fibers producing a high RL signal, such as Ce-, Ge- and Al-doped samples in our study, could also be suited for radiation monitoring applications such as beam loss monitoring for medical applications, were TID is typically much lower than the extents tested in this study. In applications demanding higher TID, occurrence of RIA could again be a factor limiting the performance of such fibers.

Also, we demonstrated that F-doped fibers, combining a low RIA sensitivity and a low production of RL signal, are well suited to be used as transport fibers for RL applications at high TID. The fact, however, that they deliver a non-null RL signal still needs to be taken into account.

Further studies of the radioluminescence properties of OFs with commonly available dopants could include a more thorough study of the physical processes of generation or conversion of RL-producing defects as well as influence of temperature, in order to evaluate the sensitivity of these elements to duration and conditions of use.

Evaluation of changes in the RL properties of OFs under other sources of irradiations, such as gamma, protons or neutrons could also be investigated to assert whether they may be used as a reliable means to detect and quantify all kinds of radiation. In the particular case of protons, the effects of Cherenkov radiation on the signal could be evaluated.

Finally, a suitable modeling of RIA effects on RL may deliver more insights about the physical processes leading to the observed decrease of the RL signal at higher doses.

References

[1] S. Girard *et al.*, "Overview of radiation induced point defects in silica-based optical fibers," *Reviews in Physics*, vol. 4, p. 100032, Nov. 2019, doi: 10.1016/j.revip.2019.100032.

[2] S. O'Keeffe, C. Fitzpatrick, E. Lewis, and A. I. Al-Shamma'a, "A review of optical fibre radiation dosimeters," *Sensor Review*, vol. 28, no. 2, pp. 136–142, Jan. 2008, doi: 10.1108/02602280810856705.

[3] N. Al Helou *et al.*, "Radioluminescence and Optically Stimulated Luminescence Responses of a Cerium-Doped Sol-Gel Silica Glass Under X-Ray Beam Irradiation," *IEEE Transactions on Nuclear Science*, vol. 65, no. 8, pp. 1591–1597, Aug. 2018, doi: 10.1109/TNS.2017.2787039.

[4] A. Vedda *et al.*, "Ce3+-doped fibers for remote radiation dosimetry," *Appl. Phys. Lett.*, vol. 85, no. 26, pp. 6356–6358, Dec. 2004, doi: 10.1063/1.1840127.

[5] C. Hoehr *et al.*, "Potential of Novel Optical Fibers for Proton Therapy Dosimetry," in *2017 IEEE Nuclear Science Symposium and Medical Imaging Conference (NSS/MIC)*, Oct. 2017, pp. 1433–1434. doi: 10.1109/NSSMIC.2017.8532703.

[6] J. Bahout *et al.*, "Cu/Ce-co-Doped Silica Glass as Radioluminescent Material for Ionizing Radiation Dosimetry," *Materials*, vol. 13, no. 11, p. 2611, Jan. 2020, doi: 10.3390/ma13112611.

[7] D. A. Bradley *et al.*, "Towards the development of doped silica radioluminescence dosimetry," *Radiation Physics and Chemistry*, vol. 154, pp. 46–52, Jan. 2019, doi: 10.1016/j.radphyschem.2018.04.019.

[8] S. Girard *et al.*, "Radiation Effects on Silica-Based Preforms and Optical Fibers—I: Experimental Study With Canonical Samples," *IEEE Transactions on Nuclear Science*, vol. 55, no. 6, pp. 3473–3482, Dec. 2008, doi: 10.1109/TNS.2008.2007297.

[9] A. V. Ishchenko *et al.*, "Radiation optical effects in commercial SiO2:Ge fibers," *J. Phys.: Conf. Ser.*, vol. 552, p. 012036, Nov. 2014, doi: 10.1088/1742-6596/552/1/012036.

[10] I. Reghioua *et al.*, "Cathodoluminescence Characterization of Point Defects in Optical Fibers," *IEEE Transactions on Nuclear Science*, vol. 64, no. 8, pp. 2318–2324, Aug. 2017, doi: 10.1109/TNS.2016.2644981.

[11] A. K. M. Mizanur Rahman *et al.*, "Germanium-doped optical fiber for real-time radiation dosimetry," *Radiation Physics and Chemistry*, vol. 116, pp. 170–175, Nov. 2015, doi: 10.1016/j.radphyschem.2015.04.018.

[12] A. K. M. M. Rahman *et al.*, "Ge-doped silica optical fibres as RL/OSL dosimeters for radiotherapy dosimetry," *Sensors and Actuators A: Physical*, vol. 264, pp. 30–39, Sep. 2017, doi: 10.1016/j.sna.2017.07.038.

[13] A. Basaif *et al.*, "Ge-doped silica optical fibre for Time Resolved Radiation Dosimetry," *Radiation Physics and Chemistry*, vol. 189, p. 109669, Dec. 2021, doi: 10.1016/j.radphyschem.2021.109669.

[14] M. Benabdesselam, F. Mady, and S. Girard, "Assessment of Ge-doped optical fibre as a TL-mode detector," *Journal of Non-Crystalline Solids*, vol. 360, pp. 9–12, Jan. 2013, doi: 10.1016/j.jnoncrysol.2012.10.016.

[15] M. Benabdesselam *et al.*, "Performance of Ge-Doped Optical Fiber as a Thermoluminescent Dosimeter," *IEEE Transactions on Nuclear Science*, vol. 60, no. 6, pp. 4251–4256, Dec. 2013, doi: 10.1109/TNS.2013.2284289.

[16] M. Benabdesselam, F. Mady, J. B. Duchez, Y. Mebrouk, and S. Girard, "The Opposite Effects of the Heating Rate on the TSL Sensitivity of Ge-doped Fiber and TLD500 Dosimeters," *IEEE Transactions on Nuclear Science*, vol. 61, no. 6, pp. 3485–3490, Dec. 2014, doi: 10.1109/TNS.2014.2354512.

[17] S. Girard, Y. Ouerdane, C. Marcandella, A. Boukenter, S. Quenard, and N. Authier, "Feasibility of radiation dosimetry with phosphorus-doped optical fibers in the ultraviolet and visible domain," *Journal of Non-*

Crystalline Solids, vol. 357, no. 8, pp. 1871–1874, Apr. 2011, doi: 10.1016/j.jnoncrysol.2010.11.113.
[18] D. A. Bradley *et al.*, "Radioluminescence sensing of radiology exposures using P-doped silica optical fibres," *Applied Radiation and Isotopes*, vol. 141, pp. 176–181, Nov. 2018, doi: 10.1016/j.apradiso.2018.02.025.
[19] W. J. Miniscalco, "Erbium-doped glasses for fiber amplifiers at 1500 nm," *Journal of Lightwave Technology*, vol. 9, no. 2, pp. 234–250, Feb. 1991, doi: 10.1109/50.65882.
[20] C. Campanella *et al.*, "Combined Temperature and Radiation Effects on Radiation-Sensitive Single-Mode Optical Fibers," *IEEE Transactions on Nuclear Science*, vol. 67, no. 7, pp. 1643–1649, Jul. 2020, doi: 10.1109/TNS.2020.2982280.
[21] I. Reghioua, "Cathodoluminescence characterization study of point defects in silica-based materials : optical fibers and nanoparticles," These de doctorat, Lyon, 2018. Accessed: Oct. 06, 2021. [Online]. Available: https://www.theses.fr/2018LYSES002
[22] S. Girard *et al.*, "Recent advances in radiation-hardened fiber-based technologies for space applications," *J. Opt.*, vol. 20, no. 9, p. 093001, Aug. 2018, doi: 10.1088/2040-8986/aad271.
[23] A. Darafsheh, R. Taleei, A. Kassaee, and J. C. Finlay, "Proton therapy dosimetry using the scintillation of the silica fibers," *Opt. Lett., OL*, vol. 42, no. 4, pp. 847–850, Feb. 2017, doi: 10.1364/OL.42.000847.
[24] J. Bahout *et al.*, "Remote Measurements of X-Rays Dose Rate Using a Cerium-Doped Air-Clad Optical Fiber," *IEEE Transactions on Nuclear Science*, vol. 67, no. 7, pp. 1658–1662, Jul. 2020, doi: 10.1109/TNS.2020.2972043.
[25] M. Cieslikiewicz-Bouet *et al.*, "Investigation of the Incorporation of Cerium Ions in MCVD-Silica Glass Preforms for Remote Optical Fiber Radiation Dosimetry," *Sensors*, vol. 21, no. 10, p. 3362, Jan. 2021, doi: 10.3390/s21103362.
[26] N. Kerboub *et al.*, "Temperature Effect on the Radioluminescence of Cu-, Ce-, and CuCe-Doped Silica-Based Fiber Materials," *IEEE Transactions on Nuclear Science*, vol. 68, no. 8, pp. 1782–1787, Aug. 2021, doi: 10.1109/TNS.2021.3075481.
[27] I. Reghioua *et al.*, "Cathodoluminescence investigation of Ge-point defects in silica-based optical fibers," *Journal of Luminescence*, vol. 179, pp. 1–7, Nov. 2016, doi: 10.1016/j.jlumin.2016.06.041.
[28] A. Alessi *et al.*, "Coupled irradiation-temperature effects on induced point defects in germanosilicate optical fibers," *J Mater Sci*, vol. 52, no. 18, pp. 10697–10708, Sep. 2017, doi: 10.1007/s10853-017-1244-x.
[29] P. J. Alonso, L. E. Halliburton, E. E. Kohnke, and R. B. Bossoli, "X-ray-induced luminescence in crystalline SiO2," *Journal of Applied Physics*, vol. 54, no. 9, p. 5369, Jun. 1998, doi: 10.1063/1.332715.
[30] M. A. Stevens-Kalceff, "Cathodoluminescence microanalysis of silica and amorphized quartz," *Miner Petrol*, vol. 107, no. 3, pp. 455–469, Jun. 2013, doi: 10.1007/s00710-013-0275-5.
[31] E. Vano *et al.*, "Dosimetric Quantities and Effective Dose in Medical Imaging: A Summary for Medical Doctors," *Insights Imaging*, vol. 12, no. 1, p. 99, Jul. 2021, doi: 10.1186/s13244-021-01041-2.